

Investigation on microstructure and mechanical properties of short-carbon-fiber/ Ti_3SiC_2 composites

Guangqi He (✉ hegq0727@163.com)

northeastern university <https://orcid.org/0000-0001-9700-8209>

Rongxiu Guo

School of Materials Science and Engineering, Northeastern University

Meishuan Li

Shenyang National Laboratory for Materials Sciences Chinese Academy of Sciences

Yang Yang

Shenyang National Laboratory for Materials Sciences Chinese Academy of Sciences

Linshan Wang

College of Science, Northeastern University

Yuhai Qian

Shenyang National Laboratory for Materials Sciences Chinese Academy of Sciences

Jun Zuo

Shenyang National Laboratory for Materials Sciences Chinese Academy of Sciences

Jingjun Xu

Shenyang National Laboratory for Materials Sciences Chinese Academy of Sciences

Changsheng Liu

School of Materials Science and Engineering, Northeastern University

Comments and reply

Keywords: Ti_3SiC_2 , short-carbon-fibers, spark-plasma-sintering, microstructure, mechanical properties

Posted Date: July 15th, 2020

DOI: <https://doi.org/10.21203/rs.3.rs-20282/v3>

License:  This work is licensed under a Creative Commons Attribution 4.0 International License.

[Read Full License](#)

Abstract

In this paper, short-carbon-fibers (C_{sf}) reinforced Ti_3SiC_2 matrix composites (C_{sf}/Ti_3SiC_2 , the C_{sf} content was 0, 2, 5 and 10 vol.%) were fabricated by spark-plasma-sintering (SPS) using Ti_3SiC_2 powders and C_{sf} as starting materials at 1300 °C. The effects of C_{sf} addition on the phase compositions, microstructures and mechanical properties (including hardness, flexural strength and fracture toughness) of C_{sf}/Ti_3SiC_2 composites were investigated. The C_{sf} , with a bi-layered transition layers, i.e. TiC and SiC layer, were homogeneously distributed in the as-prepared C_{sf}/Ti_3SiC_2 composites. With the increase of C_{sf} content, the fracture toughness of C_{sf}/Ti_3SiC_2 composites increased, but the flexural strength decreased, while the Vickers hardness decreased initially then increased steadily when the C_{sf} content was higher than 2 vol.%. These changed performances could be attributed to the introduction of C_{sf} and the formation of much stronger interfacial phases.

Introduction

Ti_3SiC_2 , a typical member of the MAX phase family, is a ternary layered compound. It has attracted extensive attention for its unique combination of metals and ceramics properties, such as low density, easy machinability, high melting point, high tensile strength and damage tolerance, excellent thermal shock resistance, good chemical stability and oxidation resistance (below 900 °C) [1-7]. Therefore, Ti_3SiC_2 is a potential structural material for the applications in the environments of high temperature, oxidation, corrosion and wear etc. [1, 2, 7, 8]. However, low fracture toughness and hardness limit its practical applications. The introduction of secondary phase as reinforcement into Ti_3SiC_2 has been proved to be an effective approach to overcome these disadvantages. For example, numerous reinforcements, including TiB_2 [9], SiC [10], c-BN [11], TiC [12], Al_2O_3 [13] and ZrO_2 [14], have been introduced to improve the mechanical properties of Ti_3SiC_2 . Commonly, the additions of ceramic particles can improve Vickers hardness and flexural strength of Ti_3SiC_2 matrix composites. For example, Górný et al. [9] reported that the addition of TiB_2 could effectively improve the Vickers hardness and elastic modulus of Ti_3SiC_2 . Tian et al. [12] prepared Ti_3SiC_2 -TiC composites and found that the Vickers hardness of the composite increased with increasing TiC content up to 90 vol.%, the flexural strength was enhanced by 64% when the content of TiC was 50 vol.%. Wang et al. [13] fabricated Ti_3SiC_2 - xAl_2O_3 ($x= 0$ -20 vol.%) composites by spark-plasma-sintering (SPS), found that Ti_3SiC_2 -20 vol.% Al_2O_3 exhibited the highest Vickers hardness, while other mechanical properties deteriorated because of the aggregation of Al_2O_3 in the composite. On the other hand, the toughness of Ti_3SiC_2 matrix composites has hardly ever been strengthened due to intrinsic brittleness of these ceramic phases.

Carbon fibers, with numerous attractively comprehensive properties, such as low density, high strength and modulus, excellent chemical inertness and small thermal expansion coefficient, are considered to be the most promising reinforcing phase for many structural ceramics [15-17]. Especially, short-carbon-fibers (C_{sf}) have been applied extensively in the preparation of ceramic matrix composites by using SPS or hot-

pressing (HP), due to their low cost, easy to add, and chemical inert at high temperatures. Interestingly, C_{sf} reinforced ceramic matrix composites usually possess relatively higher fracture toughness. For example, Wang et. al. [18] fabricated C_{sf} (up to 1 wt.%) reinforced B_4C composites, and found that the composites had higher fracture toughness compared with monolithic B_4C due to the occurrence of crack deflection and bridging resulting from interface debonding between fiber and matrix. Similarly, when C_{sf} was introduced in ZrB_2 - SiC composites, the toughness of the composites was significantly improved, resulted from fiber debonding, pulling-out and bridging as well as crack deflection [19]. Unfortunately, to date, only Lagos et. al. prepared Ti_3SiC_2 - C_f composites by SPS, and processing, microstructure and thermo-mechanical properties (thermal expansion coefficient and thermal conductivity) were investigated [20], while the mechanical properties of C_{sf} reinforced Ti_3SiC_2 composites are not available.

In this work, C_{sf}/Ti_3SiC_2 composites (the content of C_{sf} was 0, 2, 5 and 10 vol.%) were fabricated by using SPS technique. The interfacial microstructure between C_{sf} and Ti_3SiC_2 matrix and effects of C_{sf} introduction on room-temperature mechanical properties of C_{sf}/Ti_3SiC_2 composites were systematically investigated, and the role of C_{sf} addition played in reinforcement effect was also discussed.

Experimental

2.1 Materials preparation

Ti_3SiC_2 powders (Forsman Technology Co., Beijing, China) and C_{sf} (ZLXC, Co., Cangzhou, China) were used as raw materials. The purity and mean particle size of Ti_3SiC_2 powders was 98% and 3 ~ 5 μm , respectively, and the main impurity was Al_2O_3 . The length and diameter of C_{sf} was 3 mm and 7 μm , respectively. Four C_{sf}/Ti_3SiC_2 composites with C_{sf} volume fractions of 0, 2, 5, 10% were fabricated by using SPS (SPS-30T-15-3, Chenhua (Shanghai) Technology Co., Ltd, Shanghai, China). For convenience, the composites were denoted as 2, 5 and 10 C_{sf}/Ti_3SiC_2 , accordingly.

The preparation process of C_{sf}/Ti_3SiC_2 composites is schematically illustrated in Fig. 1. Firstly, C_{sf} was dispersed into deionized water with carboxymethyl cellulose sodium (CMC-Na) as the dispersant [21]. The mass ratio of CMC-Na and C_{sf} was 1:3. Then, Ti_3SiC_2 powders were added into the as-prepared solution. After stirring with a magnetic stirrer, the slurry of Ti_3SiC_2 powders and C_{sf} was obtained. Dried in an oven, the mixed material was packed into a cylindrical graphite die. Followed that, a green body with a diameter of Φ 40 mm was obtained by cold pressing under a load of 20 MPa. Subsequently, the sintering was conducted in SPS facility. After the vacuum of 10 Pa in the sintering chamber was acquired, the green body was heated to 1300 °C, under a constant pressure of 40 MPa soaked for 8 min, and the heating rate of 50 °C/min. Then cooled to room temperature in the sintering chamber. All composites were fabricated under such identical SPS condition.

2.2 Characterizations of composition and microstructure of the composites

Determinations of actual densities of C_{sf}/Ti_3SiC_2 composites by Archimedes' method. The phase compositions were performed on a D/max-2400 X-ray diffractometer (XRD) (Rigaku, Tokyo, Japan) with a Cu K α radiation ($\lambda = 0.1542$ nm). The tube voltage was 50 kV, and the current was 100 mA. The 2θ range was ($8^\circ - 80^\circ$) with count time of 1 s per 0.02° /step. The microstructure, cross-section morphologies and fracture surfaces of the composites were performed by scanning electron microscope (SEM, Oberkochen, Germany, EHT=20.00 kV) with energy dispersive spectrometer (EDS, Oxford Instruments, UK) in vacuum.

2.3 Determinations of mechanical properties

For mechanical tests, the samples were cut into a series of bars from the as-prepared composites by electrical discharge machining. Before testing, the surfaces of all samples were sanded to 2000[#] SiC sandpaper, polished to a mirror surface with 1.0 mm diamond paste, then ultrasonically cleaned in ethanol and distilled water, finally dried.

Vickers hardness test was carried out using Vickers indenter (432SVD, WOLPERT, USA) at a load of 9.8 N for 15 s. The parallel operations were conducted for nine times, finally the mean value was obtained for each sample.

All mechanical performance tests were conducted on a universal testing machine (SANS, CMT4204, Shenzhen, China). Three samples in each group were used for the flexural strength and fracture toughness measurement.

Three-point bending tests were employed to determine flexural strength. The dimensions of rectangular samples were 3 mm \times 4 mm \times 34 mm. During tests, the crosshead speed and support span were 0.5 mm/min and 30 mm, respectively. The flexural strength (σ_f) was calculated by the following Eq. (1):

See equation 1 in the supplementary files.

Where, F (N) is maximum load, L is support span, B and W are width and height of the rectangular sample, respectively.

Four-point bending tests were employed to determine fracture toughness. The dimensions of rectangular samples were 4 mm \times 8 mm \times 34 mm. The tested bars were machined as the single-edge-notched-beam (SENB) with the depth of 4 mm and the width of 0.2 mm. During tests, the crosshead speed was 0.05 mm/min, and the inner span and outer span were 10 mm and 30 mm, respectively. The fracture toughness (K_{IC}) was calculated by the following Eqs. (2) and (3)

See equations 2 and 3 in the supplementary files.

Where, S is span distance, C is notch length, B and W are the width and height of the sample, respectively.

Results And Discussion

3.1 Phase compositions of the composites

Fig. 2 shows XRD patterns of C_{sf}/Ti_3SiC_2 composites with various volume amounts of C_{sf} . For Ti_3SiC_2 and 2 C_{sf}/Ti_3SiC_2 , main phase was identified as Ti_3SiC_2 , and a small amount of Al_2O_3 impurity could be detected as well. However, when the content of C_{sf} was increased to 5 and 10 vol.%, two impurities of TiC and SiC appeared. And, the peak intensities of TiC and SiC increased simultaneously with an increase of C_{sf} content in C_{sf}/Ti_3SiC_2 composites. In C_{sf}/Ti_3SiC_2 composites, the peaks of C_{sf} was not detected by XRD, which may be caused by the low weight content of C_{sf} in the composite (the maximum theoretical value was 4.1 wt.%) and some of fibers were consumed due to the harsh interface reaction between C_{sf} and Ti_3SiC_2 . The formation of TiC and SiC were caused mainly by the interface reaction between C_{sf} and Ti_3SiC_2 [22], which will be discussed in the following section.

3.2 Microstructures of the composites

SEM micrographs of the polished surfaces of the as-prepared Ti_3SiC_2 and C_{sf}/Ti_3SiC_2 composites are presented in Fig. 3. Minor micro-pores existed in the Ti_3SiC_2 sample (Fig. 3(a)), the black spots belong to the Al_2O_3 phase. For the C_{sf}/Ti_3SiC_2 composites (Fig. 3(b, c, d)), the black circle-like and stripe-like C_{sf} were uniformly dispersed in the gray Ti_3SiC_2 matrix, and exhibited various orientations in a three-dimensional space. Additionally, the length of C_{sf} in the Ti_3SiC_2 matrix was apparently shorter than their original length (3-5 mm). The reduction in C_{sf} length is caused by the applied pressure during sintering process or C_{sf} might hide in the inner of the samples [23]. And, no pores were found in these composites, indicating that the well dispersed C_{sf} could promote the densification of Ti_3SiC_2 matrix. The most conceivable reason is that the incorporation of C_{sf} resulted in the existence of more phase boundaries, which is beneficial to the elimination of pores. In addition, C_{sf} well dispersed in the Ti_3SiC_2 matrix also confirms the desirability of preparing such composites by this method.

To get a better understanding of the interface reaction and phase evolution, the polished cross-section morphology of 10 C_{sf}/Ti_3SiC_2 was observed by SEM, and element distribution was identified by EDS, the results are presented in Fig. 4. According to Fig. 4 (a) and (b), there were two carbon fibers, which orientation was perpendicular to the viewing plane. No pores and defects appeared at the interface zone, and a chemical reaction between C_{sf} and Ti_3SiC_2 matrix was observed. The chemical compositions of the selected zones 1-5 in Fig. 4 (b) were determined by EDS, as listed in Table 1. It was found that the interface phase with duplex structure was formed between C_{sf} and Ti_3SiC_2 matrix. Based on EDS analysis results, the inner interface layer adjacent to C_{sf} was identified as TiC, while the outer interface layer was

SiC. Such result was quite different from the results of $\text{Ti}_3\text{SiC}_2\text{-C}_f$ composites prepared by Lagos et al [20]. The main reason for the formation of the interface microstructure is that our experiment actively reduces the sintering temperature of the samples to slow down the interface reaction activity, and increases the holding time from 5 min to 8 min to increase the relative density of the $\text{C}_{\text{sf}}/\text{Ti}_3\text{SiC}_2$ composites.

The interfacial reaction mechanism can be proposed tentatively based on the above SEM observations and EDS results. Although the decomposition of Ti_3SiC_2 is affected by many factors, such as temperature, pressure, atmospheric conditions, et al, it is generally considered to be stable at a temperature of 1300 °C [24-26]. From Fig 2 and Fig 3 (a), we also confirmed that pure Ti_3SiC_2 can maintain thermal stability at about 1300 °C. Therefore, the above-mentioned phenomenon could be attributed to the environment-dependent decomposition behavior of Ti_3SiC_2 , i.e., a carbon-rich environment will promote the decomposition of Ti_3SiC_2 and transform them into $\text{TiC}_{0.67}$ and Si [26-28], as described by the reaction (4).

See equation 4 in the supplementary files.

Furthermore, carbon fibers constitute a C source whereas reaction between carbon fibers and Ti_3SiC_2 (Eq. 4) leads to the formation of a Si source. Thus, SiC formation is promoted (Eq. 5) [26], and results from out diffusion of C atoms through the formed TiC_x layer.

See equation 5 in the supplementary files.

The formation of a nearly stoichiometric TiC phase is due to the diffusion of C from the C_{sf} into the carbon vacancies of $\text{TiC}_{0.67}$, as shown in the reaction (6).

See equation 6 in the supplementary files.

As a result, a double-layered interface phases are formed. Such a double layer interface can serve as a C diffusion barrier and it prevent carbon fibers to provide a C source. Therefore, the decomposition of Ti_3SiC_2 is inhibited.

From the EDS result in Fig. 4(e), the bright agglomerates were enriched in Al. Meanwhile, the EDS analysis also confirmed the existence of minor well-dispersed Al_2O_3 particles with the size of 2-3 μm , which corresponds to the XRD results.

The actual densities of the as-prepared composites are listed in Table 2. With increasing the content of C_{sf} , the density of the composite decreased. This is because that the density of C_{sf} (1.78 g/cm^3) was much lower than that of Ti_3SiC_2 (4.53 g/cm^3). Based on the nominal ratio of the initial contents of Ti_3SiC_2 and C_{sf} , the theoretical densities of the as-prepared Ti_3SiC_2 and $\text{C}_{\text{sf}}/\text{Ti}_3\text{SiC}_2$ composites were calculated using the rule of mixtures, also listed in Table 2. Obviously, the relative densities of all

materials prepared by SPS were higher than 98% in this work. In addition, under the condition of the same SPS processing, the relative densities of the as-prepared C_{sf}/Ti_3SiC_2 composite increased with increasing C_{sf} content. It should be noted that, during the calculation of the theoretical densities of the composites, only the nominal compositions of the composite were considered, the formation of high density TiC (4.93 g/cm³ [1]) during the sintering of the bulk material was neglected. Therefore, correspondingly, the higher contents of C_{sf} as well as TiC led to the greater deviation of calculated density.

3.3 Mechanical properties of the composites

3.3.1 Vickers hardness

The dependence of Vickers hardness of Ti_3SiC_2 and C_{sf}/Ti_3SiC_2 composites on the theoretical content of C_{sf} is shown in Fig. 5. The Vickers hardness of the pristine Ti_3SiC_2 sintered by SPS in the present work was 5.40 ± 0.06 GPa (measured at the indentation load of 9.8 N). It was reported previously that the hardness of monolithic Ti_3SiC_2 was about 4 GPa [3], lower than that of Ti_3SiC_2 synthesized by SPS in this work. The reasons may be due to our Ti_3SiC_2 sample contains a small amount of Al_2O_3 phase, it may also be due to the impact of indentation size. El Raghy et al. [3] found that indentation size had a great influence on the hardness. From Fig. 5, the Vickers hardness of the composite decreased slightly for the case of 2 vol.% C_{sf} , and then increased monotonously to 6.80 ± 0.87 GPa with increasing C_{sf} content up to 10 vol.%. For a small amount of C_{sf} (2 vol.%) addition, the slightly decline of the hardness of the composite was related to C_{sf} possessing lower hardness compared to Ti_3SiC_2 matrix. The formation of minor TiC and SiC interfacial phases with the higher hardness of about 28-30 GPa [29] and 22 GPa [30] compared to Ti_3SiC_2 matrix, respectively, was insufficient to compensate the hardness loss by the introduction of C_{sf} . For the 5 C_{sf}/Ti_3SiC_2 , similar situation took place. Although the increased contents of TiC and SiC gave rise to the increased hardness of the composite, which was still lower than that of the matrix Ti_3SiC_2 . The hardness of the composite was degraded due to the chemical reaction between C_{sf} and Ti_3SiC_2 matrix, but further evaluate the content of the interface reaction products to compensate for the decrease in the hardness of the composite is beyond the scope of this paper. When the content of C_{sf} was 10 vol.%, the hardness of the as-prepared composite was 6.69 GPa, which was larger than that of the Ti_3SiC_2 . For the 10 C_{sf}/Ti_3SiC_2 , the contents of formed TiC and SiC interfacial phases with higher hardness was sufficient to compensate the hardness loss by the introduction of C_{sf} . Zhang et al. [31] presented that the maximum Vickers hardness of Ti_3SiC_2 -40 vol.% TiC composite was about 13 GPa. Accordingly, it is reasonable to believe that the contents of added C_{sf} and TiC derived from the interfacial reaction between C_{sf} and Ti_3SiC_2 simultaneously determine the hardness of C_{sf}/Ti_3SiC_2 composite.

3.3.2 Flexural strength and fracture toughness

The dependence of the flexural strength and fracture toughness of Ti_3SiC_2 and $\text{C}_{\text{sf}}/\text{Ti}_3\text{SiC}_2$ composites on the theoretical content of C_{sf} are illustrated in Fig. 6. When the content of C_{sf} increased from 0 to 10 vol.%, the flexural strength decreased from 602 ± 34 MPa to 468 ± 34 MPa. The main reason for the reduction of flexural strength is that the modulus of C_{sf} (~ 250 GPa) is lower than that of Ti_3SiC_2 matrix (~ 326 GPa), and the presence of C_{sf} in the matrix resulted in the reduced load carrying capacity of the composites [1, 19]. Meanwhile, it was also related to the formation of TiC and SiC with a high content between the matrix and C_{sf} . Both TiC and SiC formed by in-situ reaction exist in a layered structure in the matrix. The layered structure as a reinforcement is different from the particles as a reinforcement, which does not inhibit the growth of crystal grains. On the contrary, they occupy the space of the matrix and fibers, and their reinforcement effect depends on the inherent properties of TiC and SiC and interface bonding strength. The mechanical properties of both TiC and SiC are lower than those of Ti_3SiC_2 , which is main reason for the reduction of the flexural strength of composites.

It also can be clearly seen from Fig. 6 that as the increase of C_{sf} content, the fracture toughness of $\text{C}_{\text{sf}}/\text{Ti}_3\text{SiC}_2$ composites increased, reaching a maximum value of 6.48 ± 0.29 MPa $\cdot\text{m}^{1/2}$ for 10 $\text{C}_{\text{sf}}/\text{Ti}_3\text{SiC}_2$. After adding C_{sf} , the fracture toughness of $\text{C}_{\text{sf}}/\text{Ti}_3\text{SiC}_2$ composites were enhanced, which was related to the activation of certain kinds of toughening mechanisms [32, 33], as described as follows.

The mechanical properties of fiber-reinforced composites rely on not only the intrinsic properties of fiber and matrix, but also the characteristics of fiber/matrix interface [34, 35]. Interface delamination and the formation of a “weak” interphase are significantly vital to the comprehensive properties of fiber-reinforced ceramic matrix composites [36]. During the failure process of composites, their fracture toughness could be improved effectively by interface debonding, fiber bridging and fiber pulling-out caused by such characteristics mentioned above. To further understand the possible toughening mechanisms of the as-prepared C_{sf} reinforced Ti_3SiC_2 composites, the fractured surfaces of the composites after SENB test were observed by SEM, as shown in Fig. 7. Obviously, these composites exhibited a fully brittle fracture. The breakage of C_{sf} and interface debonding could be found, but fiber pull-out did not appear, corresponding to a strong interface bonding between C_{sf} and Ti_3SiC_2 . During the preparation of $\text{C}_{\text{sf}}/\text{Ti}_3\text{SiC}_2$ composites, original C_{sf} did not undergo any surface treatment. As mentioned above, the formation of interfacial phases of TiC and SiC during heat-pressing sintering caused an enhanced interface bonding between C_{sf} and Ti_3SiC_2 matrix, and such chemical bonding was much stronger than van der Waals’ force in the matrix [37, 38]. Therefore, the fiber bridging or fiber pulling-out became very difficult to occur due to the presence of strong interface between fiber reinforcement and matrix [35, 39]. On the other hand, under this condition, as the C_{sf} content increases, more energy is consumed during fracture process due to interface debonding and C_{sf} breakage, thereby resulting in the increased fracture toughness of the as-prepared composite.

Moreover, the fracture surface morphologies of Ti_3SiC_2 and 10 $\text{C}_{\text{sf}}/\text{Ti}_3\text{SiC}_2$ composite were further observed under high magnification SEM, as shown in Fig 8. For 10 $\text{C}_{\text{sf}}/\text{Ti}_3\text{SiC}_2$ composite (Fig. 8 (b)), it

clearly reveals two different fracture modes. The fracture of the unreacted Ti_3SiC_2 exhibited the same fracture mode as the pure Ti_3SiC_2 materials (Fig. 8 (a)), which was mainly characterized by grain pull-out and grain delamination. On the other hand, in the interface reaction layer, the fracture surface is relatively flat, showing a typical transgranular fracture mode. This clearly clarifies that the harsh interface reaction to form brittle compounds is not conducive to the mechanical properties of the fiber-reinforced composites [40]. In addition, the grain size of these compounds is much smaller than Ti_3SiC_2 .

Conclusions

C_{sf} reinforced Ti_3SiC_2 composites were prepared by SPS process. The behavior of C_{sf} in the as-prepared $\text{C}_{\text{sf}}/\text{Ti}_3\text{SiC}_2$ composites, microstructures and mechanical properties of the as-prepared $\text{C}_{\text{sf}}/\text{Ti}_3\text{SiC}_2$ composites were studied. The main results are as follows:

1. Dense $\text{C}_{\text{sf}}/\text{Ti}_3\text{SiC}_2$ composites with 2, 5, 10 vol.% C_{sf} were prepared by SPS at 1300° . The interfacial reaction layer with duplex structure of TiC inner layer and SiC outer layer was formed between C_{sf} and Ti_3SiC_2 matrix.
2. Among the as-prepared Ti_3SiC_2 matrix composites, the one with 10 vol.% C_{sf} exhibited the highest Vickers hardness (6.80 ± 0.87 GPa) and fracture toughness (6.48 ± 0.29 $\text{MPa}\cdot\text{m}^{1/2}$), which were increased by 36.7% and 17.8% compared with Ti_3SiC_2 , respectively. Its flexural strength was 467.7 MPa, decreased by 22.3%.
3. The contents of added C_{sf} and TiC produced by the interfacial reaction between C_{sf} and Ti_3SiC_2 matrix played a critical part in the mechanical properties of $\text{C}_{\text{sf}}/\text{Ti}_3\text{SiC}_2$.

Declarations

Acknowledgements

This work was supported by the Joint fund of Liaoning-SYNL (Grant No. 2019JH3/30100035) as well as Science and Technology Foundation of National Defense Key Laboratory (Grant No. HTKJ2019KL703006).

References

- [1] Barsoum MW. The MN+1AXN phases: A new class of solids: Thermodynamically stable nanolaminates. *Prog Solid State Chem* 2000, **28**: 201-281.
- [2] Barsoum MW, El-Raghy T. Synthesis and characterization of a remarkable ceramic: Ti_3SiC_2 . *J Am Ceram Soc* 1996, **79**: 1953-1956.

- [3] El-Raghy T, Zavaliangos A, Barsoum MW, et al. Damage Mechanisms around Hardness Indentations in Ti_3SiC_2 . *J Am Ceram Soc* 2005, **80**: 513-516.
- [4] Barsoum M, El-Raghy T. A progress report on Ti_3SiC_2 , Ti_3GeC_2 , and the H-phases, M_2BX . *J Mater Synth Process* 1997, **5**: 197-216.
- [5] Zhou Y, Sun Z, Chen S, et al. In-situ hot pressing/solid-liquid reaction synthesis of dense titanium silicon carbide bulk ceramics. *Mater Res Innovations* 1998, **2**: 142-146.
- [6] Sun Z, Zhou Y, Li M. Oxidation behaviour of Ti_3SiC_2 -based ceramic at 900-1300°C in air. *Corros Sci* 2001, **43**: 1095-1109.
- [7] Gao NF, Miyamoto Y, Zhang D. Dense Ti_3SiC_2 prepared by reactive HIP. *J Mater Sci* 1999, **34**: 4385-4392.
- [8] Ghosh NC, Harimkar SP. Phase analysis and wear behavior of in-situ spark plasma sintered Ti_3SiC_2 . *Ceram Int* 2013, **39**: 6777-6786.
- [9] Górný G, Rączka M, Stobierski L, et al. Ceramic composite Ti_3SiC_2 - TiB_2 Microstructure and mechanical properties. *Mater Charact* 2009, **60**: 1168-1174.
- [10] Li S-B, Xie J-X, Zhang L-T, et al. Mechanical properties and oxidation resistance of $\text{Ti}_3\text{SiC}_2/\text{SiC}$ composite synthesized by in situ displacement reaction of Si and TiC. *Mater Lett* 2003, **57**: 3048-3056.
- [11] Benko E, Klimczyk P, Mackiewicz S, et al. cBN- Ti_3SiC_2 composites. *Diam Relat Mater* 2004, **13**: 521-525.
- [12] Tian W, Sun Z, Hashimoto H, et al. Synthesis, microstructure and mechanical properties of Ti_3SiC_2 -TiC composites pulse discharge sintered from Ti/Si/TiC powder mixture. *Mater Sci Eng, A* 2009, **526**: 16-21.
- [13] Wang HJ, Jin ZH, Miyamoto Y. Effect of Al_2O_3 on mechanical properties of $\text{Ti}_3\text{SiC}_2/\text{Al}_2\text{O}_3$ composite. *Ceram Int* 2002, **28**: 931-934.
- [14] Shi SL, Pan W. Toughening of Ti_3SiC_2 with 3Y-TZP addition by spark plasma sintering. *Mater Sci Eng, A* 2007, **447**: 303-306.
- [15] Hou LG, Wu RZ, Wang XD, et al. Microstructure, mechanical properties and thermal conductivity of the short carbon fiber reinforced magnesium matrix composites. *J Alloys compd* 2017, **695**: 2820-2826.
- [16] Li S, Zhang Y, Han J, et al. Effect of carbon particle and carbon fiber on the microstructure and mechanical properties of short fiber reinforced reaction bonded silicon carbide composite. *J Eur Ceram Soc* 2013, **33**: 887-896.

- [17] Hong W, Gui K, Hu P, et al. Preparation and characterization of high-performance $ZrB_2-SiC-C_f$ composites sintered at 1450 °C. *J Adv Ceram* 2017, **6**: 110-119.
- [18] Wang M, Zhang Z, Sun Z, et al. Effect of fiber type on mechanical properties of short carbon fiber reinforced B_4C composites. *Ceram Int* 2009, **35**: 1461-1466.
- [19] Yang F, Zhang X, Han J, et al. Characterization of hot-pressed short carbon fiber reinforced ZrB_2-SiC ultra-high temperature ceramic composites. *J Alloys compd* 2009, **472**: 395-399.
- [20] Lagos MA, Pellegrini C, Agote I, et al. Ti_3SiC_2-Cf composites by spark plasma sintering: Processing, microstructure and thermo-mechanical properties. *J Eur Ceram Soc* 2019, **39**: 2824-2830.
- [21] Tang C, Li T, Gao J, et al. Microstructure and mechanical behavior of the Cf/Ti_3SiC_2-SiC composites fabricated by compression molding and pressureless sintering. *Ceram Int* 2017, **43**: 16204-16209.
- [22] Zhou X, Yang H, Chen F, et al. Joining of carbon fiber reinforced carbon composites with Ti_3SiC_2 tape film by electric field assisted sintering technique. *Carbon* 2016, **102**: 106-115.
- [23] Gui K, Liu F, Wang G, et al. Microstructural evolution and performance of carbon fiber-toughened ZrB_2 ceramics with SiC or $ZrSi_2$ additive. *J Adv Ceram* 2018, **7**: 343-351.
- [24] Qin J, He D. Phase stability of Ti_3SiC_2 at high pressure and high temperature. *Ceram Int* 2013, **39**: 9361-9367.
- [25] Sun Z, Zhou J, Music D, et al. Phase stability of Ti_3SiC_2 at elevated temperatures. *Scripta Mater* 2006, **54**: 105-107.
- [26] Racault C, Langlais F, Naslain R. Solid-state synthesis and characterization of the ternary phase Ti_3SiC_2 . *J Mater Sci* 1994, **29**: 3384-3392.
- [27] El-Raghy T, Barsoum MW. Diffusion kinetics of the carburization and silicidation of Ti_3SiC_2 . *J Appl Phys* 1998, **83**: 112-119.
- [28] Gao N, Miyamoto Y, Zhang D. On physical and thermochemical properties of high-purity Ti_3SiC_2 . *Mater Lett* 2002, **55**: 61-66.
- [29] Ghosh NC, Harimkar SP. Microstructure and wear behavior of spark plasma sintered Ti_3SiC_2 and Ti_3SiC_2-TiC composites. *Ceram Int* 2013, **39**: 4597-4607.
- [30] Yin XW, Cheng LF, Zhang LT, et al. Fibre-reinforced multifunctional SiC matrix composite materials. *Int Mater Rev* 2016, **62**: 117-172.

- [31] Zhang J, Wang L, Jiang W, et al. Effect of TiC content on the microstructure and properties of Ti_3SiC_2 -TiC composites in situ fabricated by spark plasma sintering. *Mater Sci Eng, A* 2008, **487**: 137-143.
- [32] Karimirad S, Balak Z. Characteristics of spark plasma sintered ZrB_2 -SiC-SCFs composites. *Ceram Int* 2019, **45**: 6275-6281.
- [33] Shahedi Asl M. Microstructure, hardness and fracture toughness of spark plasma sintered ZrB_2 -SiC- C_f composites. *Ceram Int* 2017, **43**: 15047-15052.
- [34] Brennan JJ, McCarthy G. Interfacial studies of refractory glass-ceramic matrix/advanced SiC-fiber reinforced composites. *Mater Sci Eng, A* 1993, **162**: 53-72.
- [35] He X, Guo Y, Yu Z, et al. Study on microstructures and mechanical properties of short-carbon-fiber-reinforced SiC composites prepared by hot-pressing. *Mater Sci Eng, A* 2009, **527**: 334-338.
- [36] Arai Y, Inoue R, Goto K, et al. Carbon fiber reinforced ultra-high temperature ceramic matrix composites: A review. *Ceram Int* 2019, **45**: 14481-14489.
- [37] Wang C, Chen L, Li J, et al. Enhancing the interfacial strength of carbon fiber reinforced epoxy composites by green grafting of poly (oxypropylene) diamines. *Composites Part A* 2017, **99**: 58-64.
- [38] Sun J, Zhao F, Yao Y, et al. High efficient and continuous surface modification of carbon fibers with improved tensile strength and interfacial adhesion. *Appl Surf Sci* 2017, **412**: 424-435.
- [39] Yang WS, Biamino S, Padovano E, et al. Microstructure and mechanical properties of short carbon fibre/SiC multilayer composites prepared by tape casting. *Composites Sci Technol* 2012, **72**: 675-680.
- [40] Guo S, Hu C, Gao H, et al. SiC(SCS-6) fiber-reinforced Ti_3AlC_2 matrix composites: Interfacial characterization and mechanical behavior. *J Eur Ceram Soc* 2015, **35**: 1375-1384.

Tables

Table 1 EDS results of the marked spots 1-5 in Fig 4(b).

Marked zone	Compositions (atomic %)					Corresponding phase
	Ti	Si	Al	C	O	
1	6.81±2.07	2.36±3.27	0.40±7.50	90.42±6.65	-	C_{sf}
2	50.93±1.42	3.84±5.19	1.10±9.71	44.13±8.27	-	TiC
3	5.23±1.65	57.71±4.27	0.79±5.26	36.27±10.46	-	SiC
4	45.56±1.45	15.34±4.48	0.59±12.67	38.51±9.48	-	Ti_3SiC_2
5	2.67±1.67	1.36±6.65	26.21±4.71	23.68±10.89	46.09±9.42	Al_2O_3

Table 2 The determined and calculated densities of the as-prepared Ti_3SiC_2 and $\text{C}_{sf}/\text{Ti}_3\text{SiC}_2$ composites.

Nominal compositions (vol %)	Apparent density (g cm^{-3})	Theoretical density (g cm^{-3})	Relative density (%)
Ti_3SiC_2	4.45	4.53	98.2
2 $\text{C}_{\text{sf}}/\text{Ti}_3\text{SiC}_2$	4.41 ± 0.01	4.47	98.6
5 $\text{C}_{\text{sf}}/\text{Ti}_3\text{SiC}_2$	4.35 ± 0.01	4.39	99.1
10 $\text{C}_{\text{sf}}/\text{Ti}_3\text{SiC}_2$	4.24 ± 0.01	4.25	99.8

Figures

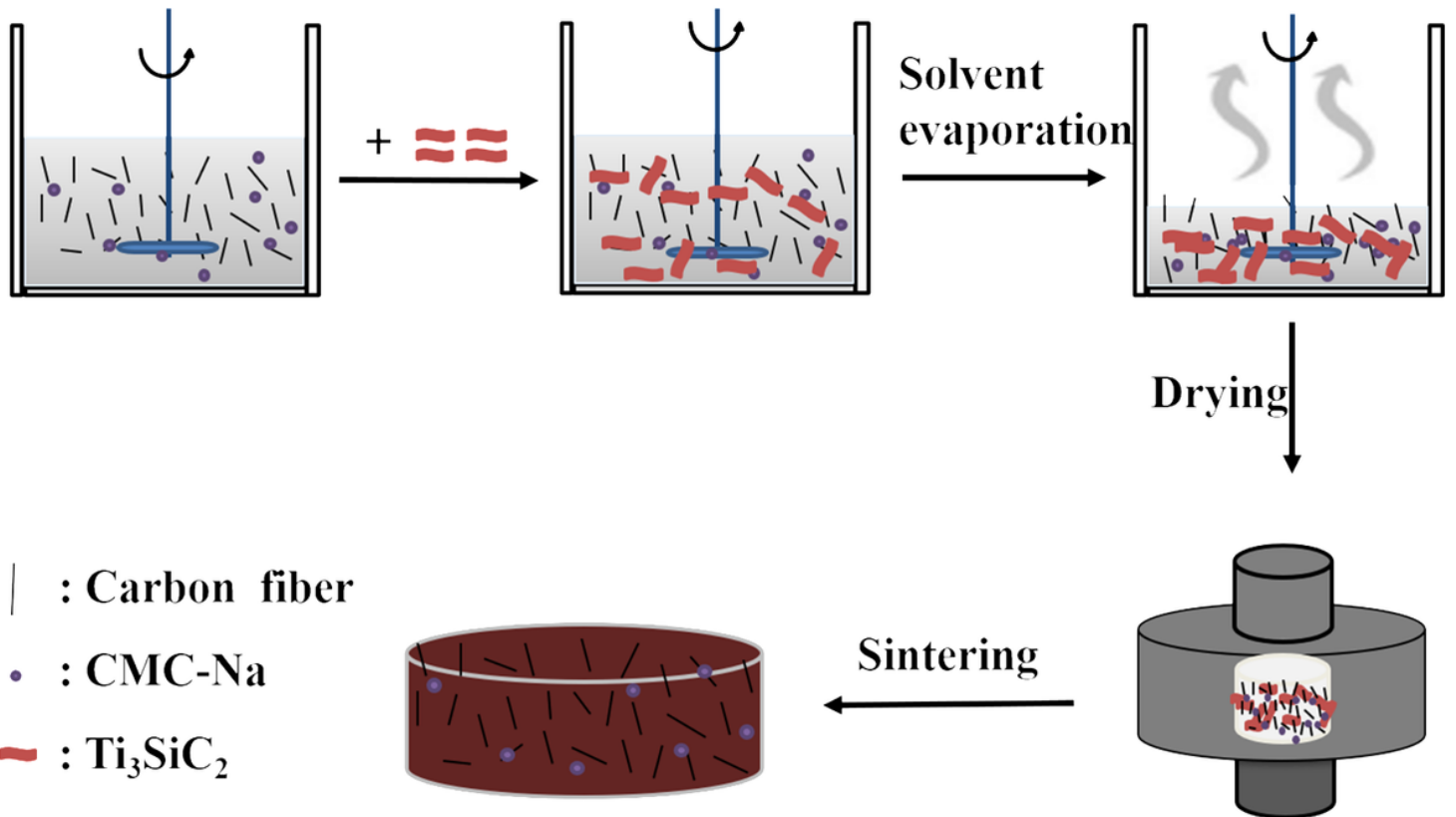


Figure 1

Schematic illustrations of the preparation process of $\text{Csf}/\text{Ti}_3\text{SiC}_2$ composites by using SPS.

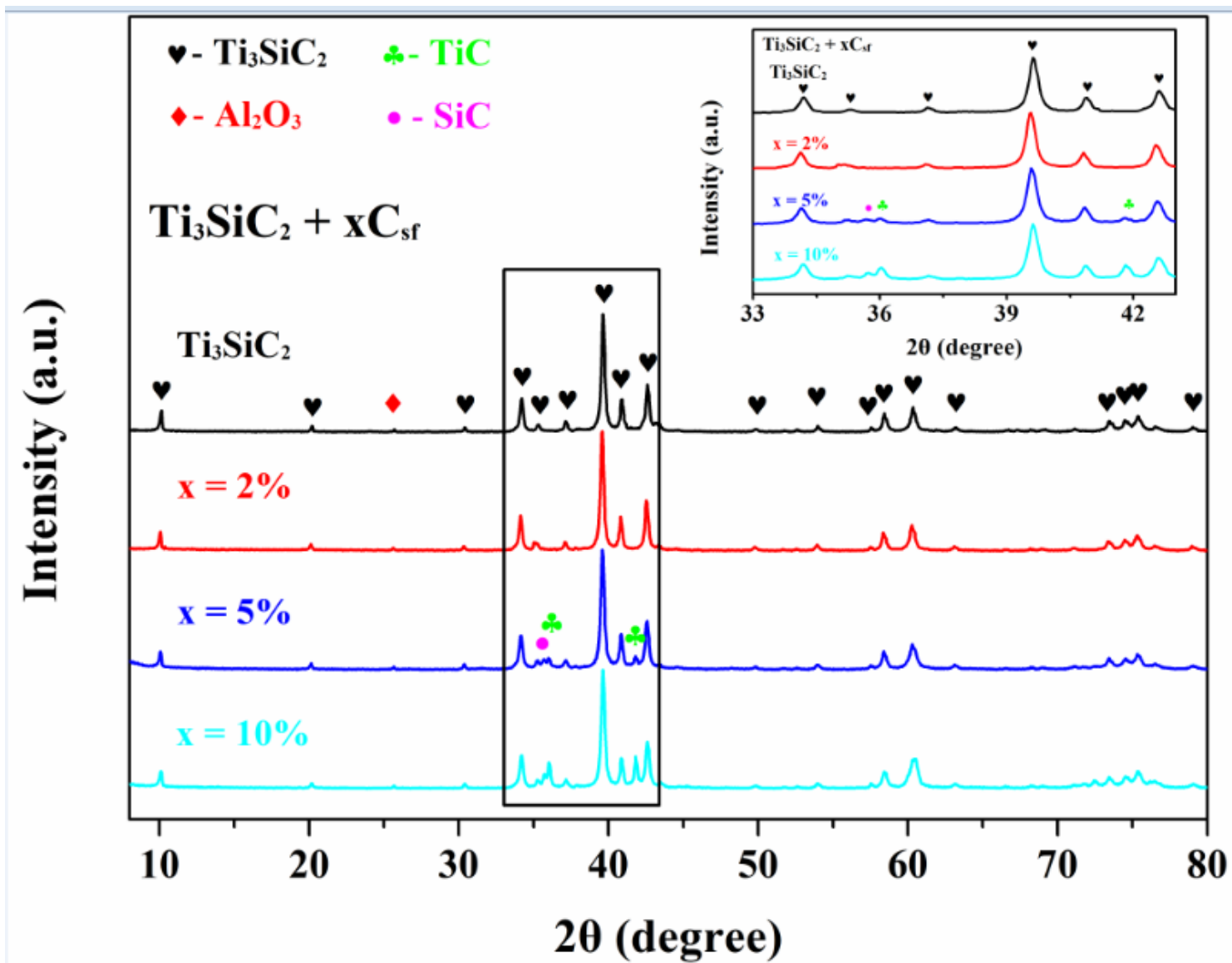


Figure 2

XRD patterns of Csf/ Ti_3SiC_2 composites with the different contents of Csf. The inset shows the enlarged views in the 2θ range of 33o-43o.

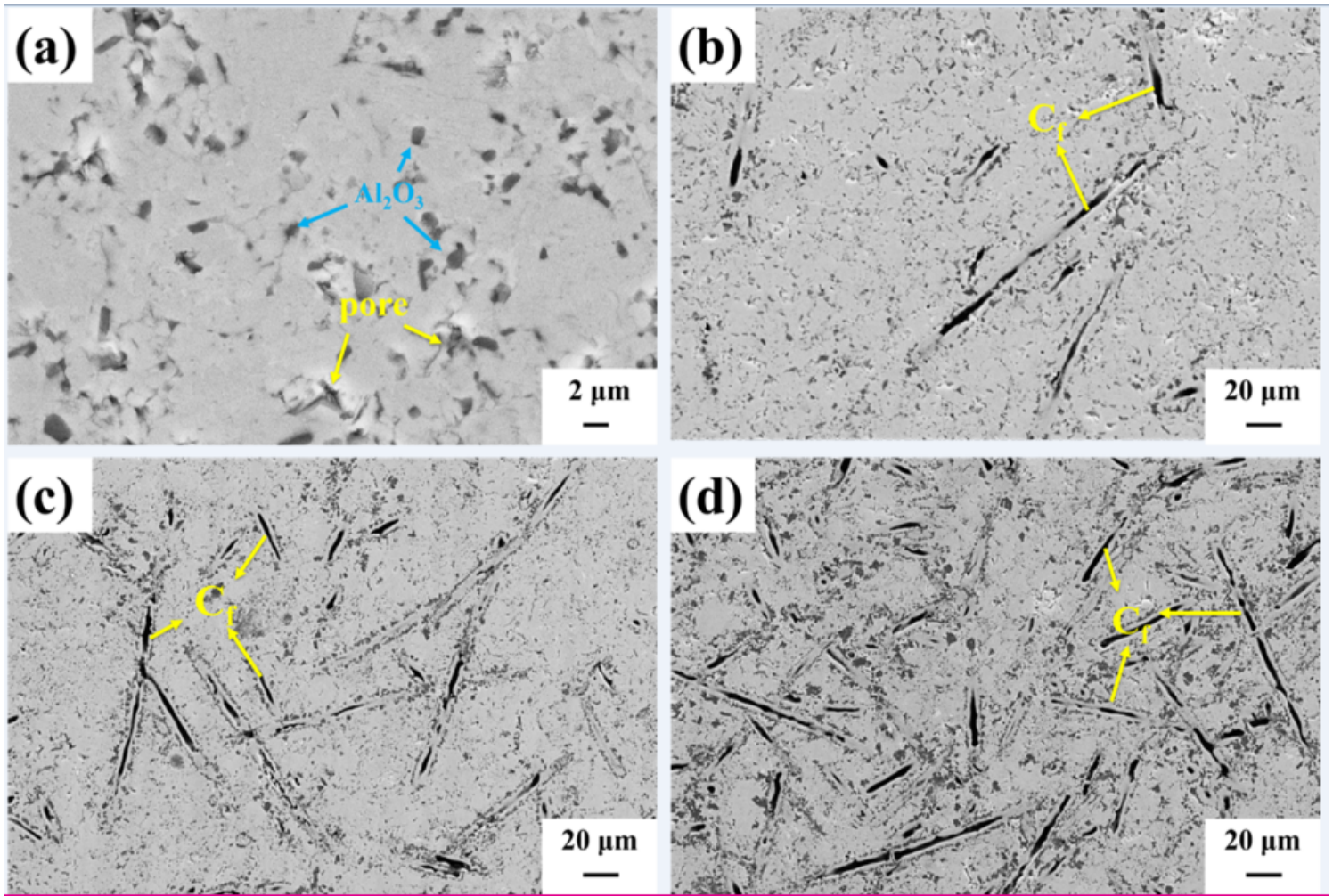


Figure 3

SEM micrographs of the polished surfaces of (a) Ti_3SiC_2 , (b) 2 CsF/ Ti_3SiC_2 , (c) 5 CsF/ Ti_3SiC_2 and (d) 10 CsF/ Ti_3SiC_2 .

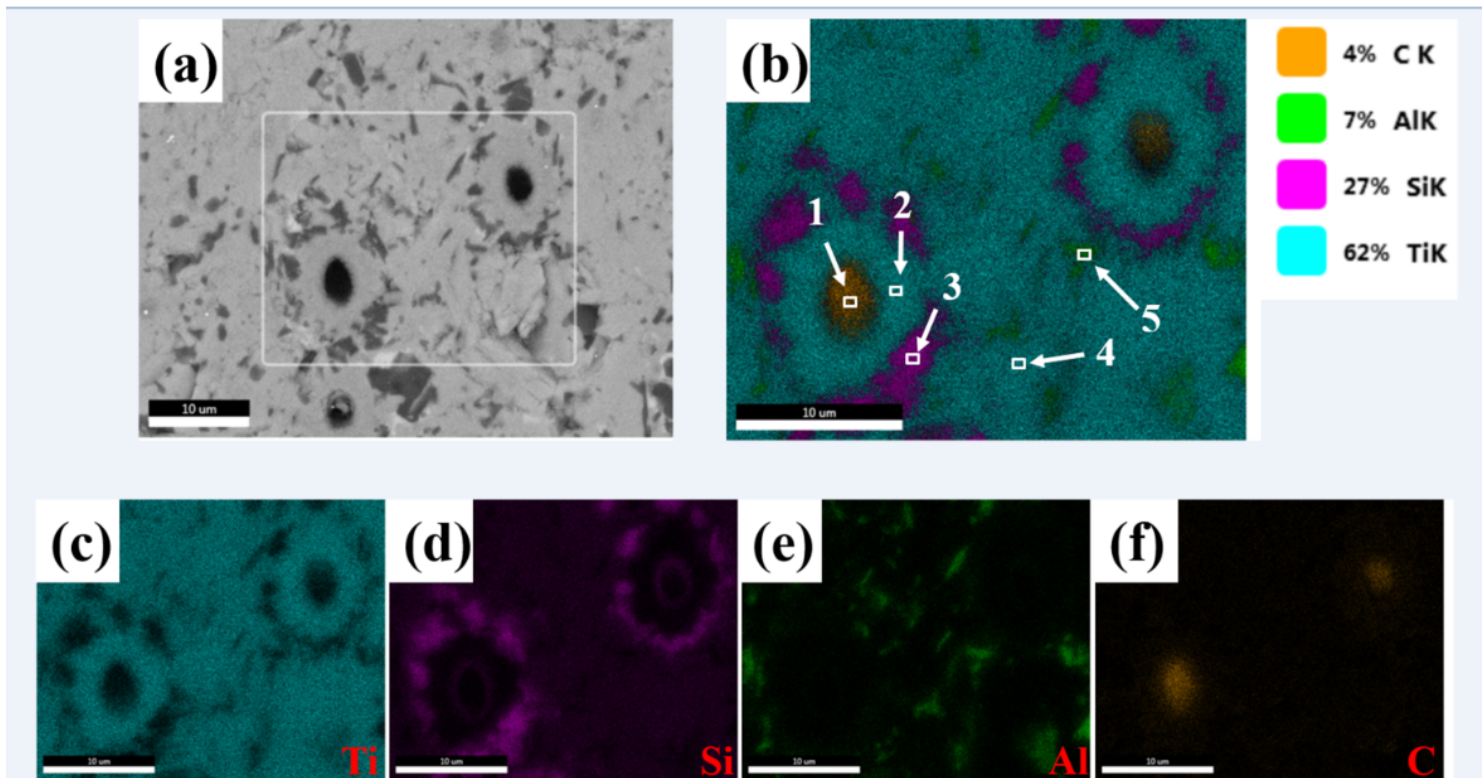


Figure 4

(a) SEM image of polished cross section of 10 Csf/Ti₃SiC₂; (b) element mappings in the white frame area in Fig. 4 (a); element distributions of (c) Ti, (d) Si, (e) Al, and (f) C.

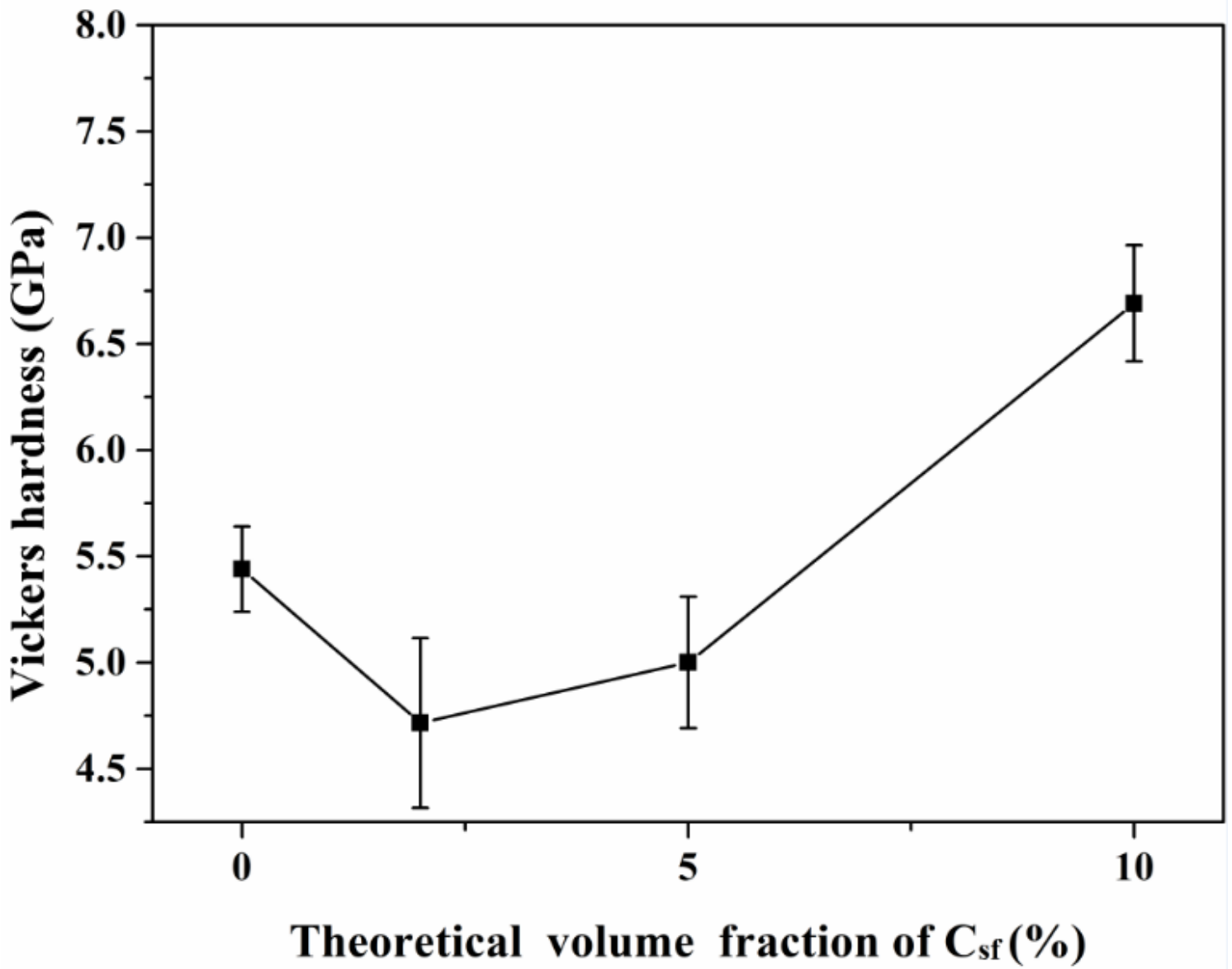


Figure 5

The dependence of Vickers hardness of the as-prepared Csf/Ti₃SiC₂ composites on the content of Csf.

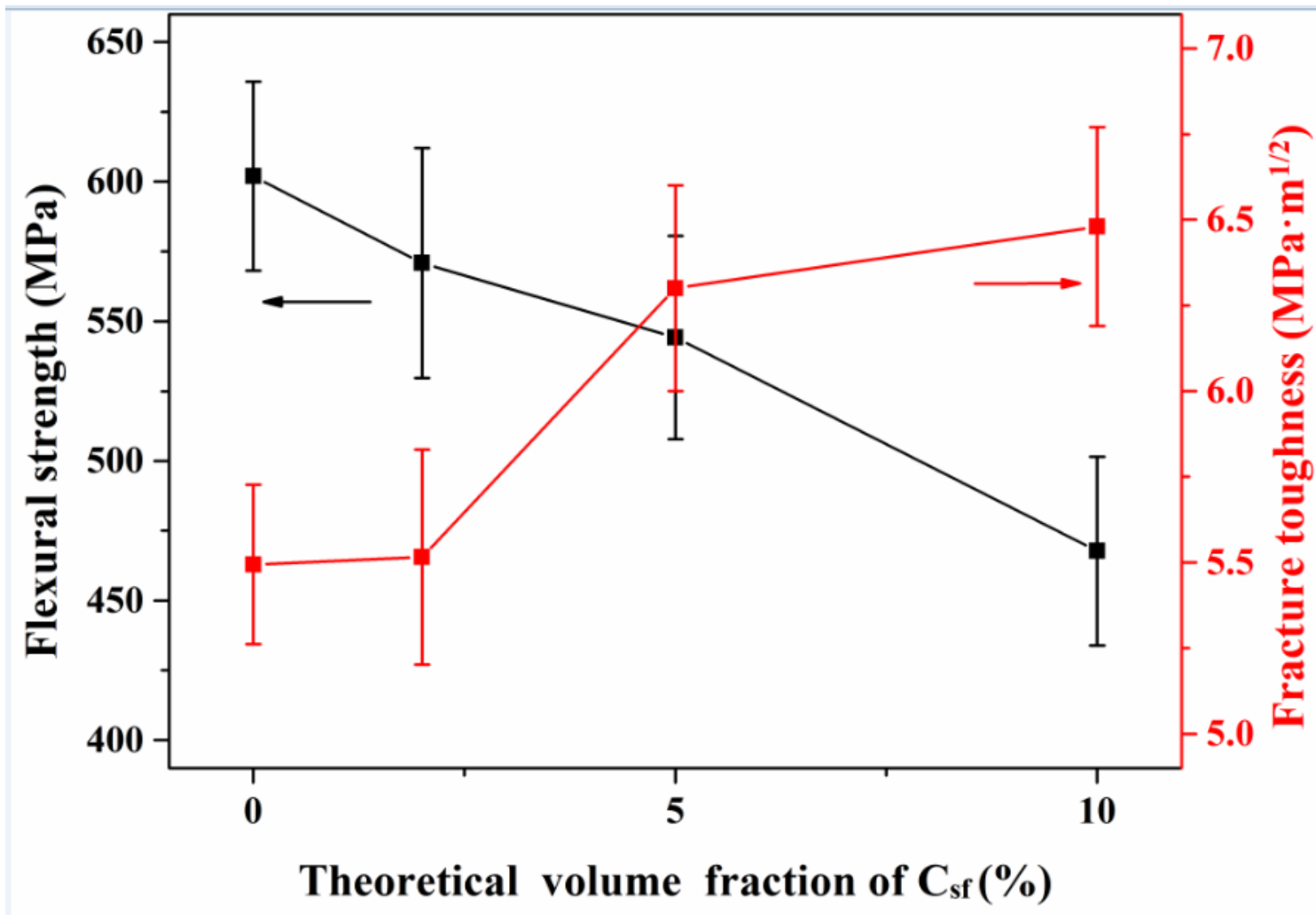


Figure 6

The dependence of flexural strength and fracture toughness of the as-prepared Csf/Ti₃SiC₂ composites on the content of Csf.

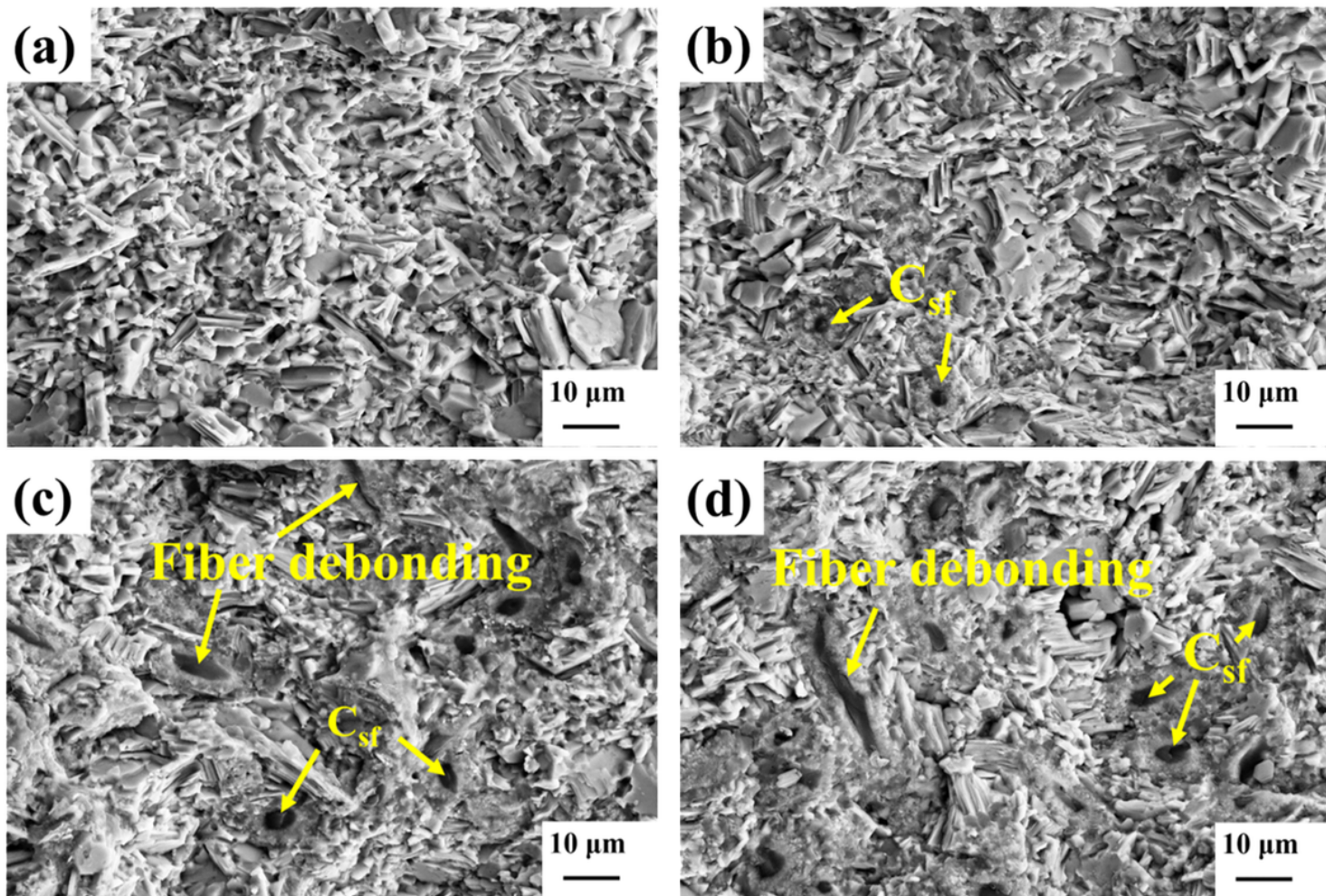


Figure 7

SEM micrographs of the fracture surfaces of (a) Ti_3SiC_2 , (b) 2 Csf/Ti_3SiC_2 , (c) 5 Csf/Ti_3SiC_2 and (d) 10 Csf/Ti_3SiC_2 .

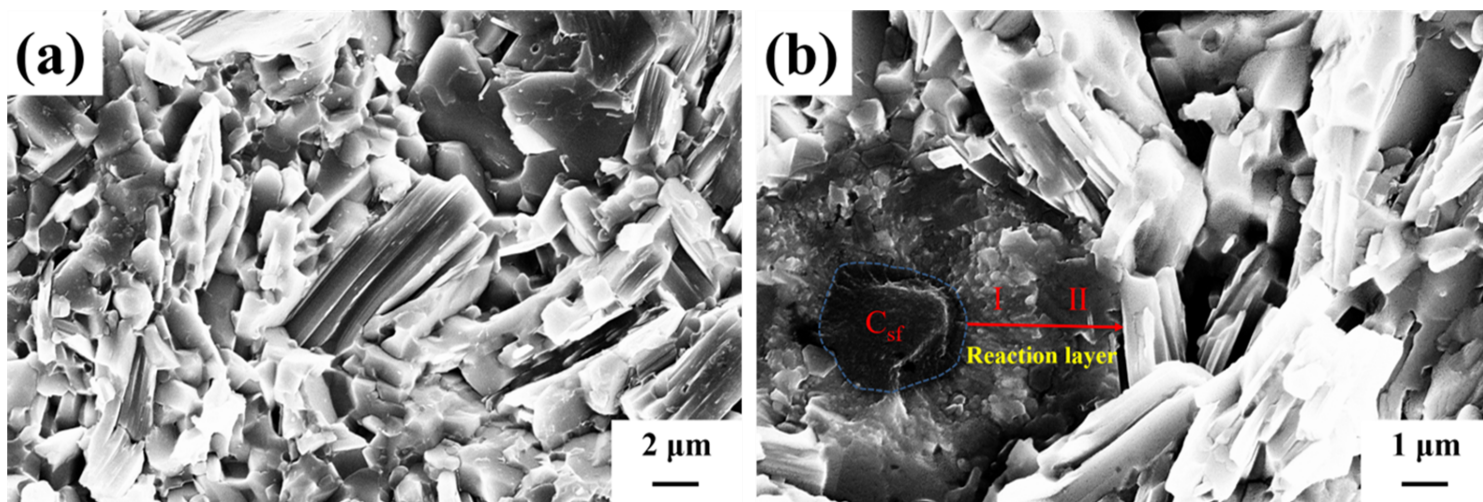


Figure 8

High magnification SEM micrographs of the fracture surfaces of (a) Ti_3SiC_2 and (b) 10 Csf/Ti_3SiC_2 .

Supplementary Files

This is a list of supplementary files associated with this preprint. Click to download.

- [equations.docx](#)